# On the gear mechanics before the cycloid and involute profiling

Francesco Sorge

*Dipartimento di Ingegneria Chimica, Gestionale, Informatica, Meccanica,*
*Università di Palermo, Italy*
*E-mail: francesco.sorge@unipa.it*

*Keywords:* Ancient machinery, gearing, trapezoid profiles.

SUMMARY. After the extraordinary development of the machinery in the Hellenistic antiquity, the gear technique was transmitted to the Middle Ages through the Byzantine and Islamic culture and then to the Modern Era. The tooth profile was very crude, often trapezoidal or even rectangular and the gear behavior differed substantially from the modern involute profile. The kinematics of trapezoid profiles is here analyzed in detail, focusing on the temporal variation of the speed ratio due to the back and forth shifting of the relative instant center. Considering an isolated tooth pair, an approach phase is firstly observable, where the tip of the driven profile is pushed by the driver flank and then, after passing through the matching configuration, a recess phase follows, where the tip of the driver profile pushes the flank of the driven one. The acceptability of each configuration of this theoretical evolution is then checked according to the interference prevention requirement for the following and preceding tooth pairs and for the back inactive profiles. This yields some limitation to the tooth thickness, which may justify the frequent tooth slenderness in the design of the gear systems of the Renaissance. The periodic tooth collisions due to the jerky variability of the speed ratio are properly analyzed, together with the energy losses arising from the sliding friction. Overall, the results show that only one tooth pair is active at each time instant and the acceptable contacts may belong to the only approach region, or to the only recess region, or may be split into two separate sub-phases, in approach and in recess, or may even straddle both regions. The occurrence of each of these situations depends on the average speed ratio and on the assigned clearance between the two wheels.

## 1 INTRODUCTION

The gear mechanisms were a rather common application of the Hellenistic manufacture and were used for astronomical devices, astrolabes and odometers. For example, the Antikythera fragments are parts of a planetary gear system with equilateral triangular tooth shape, presumably of the first century B.C., ascribable perhaps to the philosophers Posidonius or Hypparchus, both from the Academy of Rhodes. It was retrieved at the beginning of the XX century from the Antikythera wreck, which was discovered thanks to some sponge-divers anchored near the coast of the homonymous island (‘*Αντικύθηρα*, meaning "in front of Kythera", is a small Greek island with roughly one hundred inhabitants in the sea channel between Crete and the larger island of Kythera). This device has been widely studied in the recent past (for example, see Pastore [1], de Solla Price [2-3], Wright [4]) and still draws the attention of the scientific community participating in the Antikythera Mechanism Research Project [5]. However, it is amazing that some more advanced design conception is recognizable in the more ancient gear fragment of Olbia (Sardinia, Italy), probably belonging to an orrery designed by Archimedes of Syracuse (third century B.C.), whose tooth profiles appear extraordinarily close to the modern cycloidal shape [1]. It is very likely that this orrery was the one mentioned by Cicero in *De Re Publica*, which was brought to

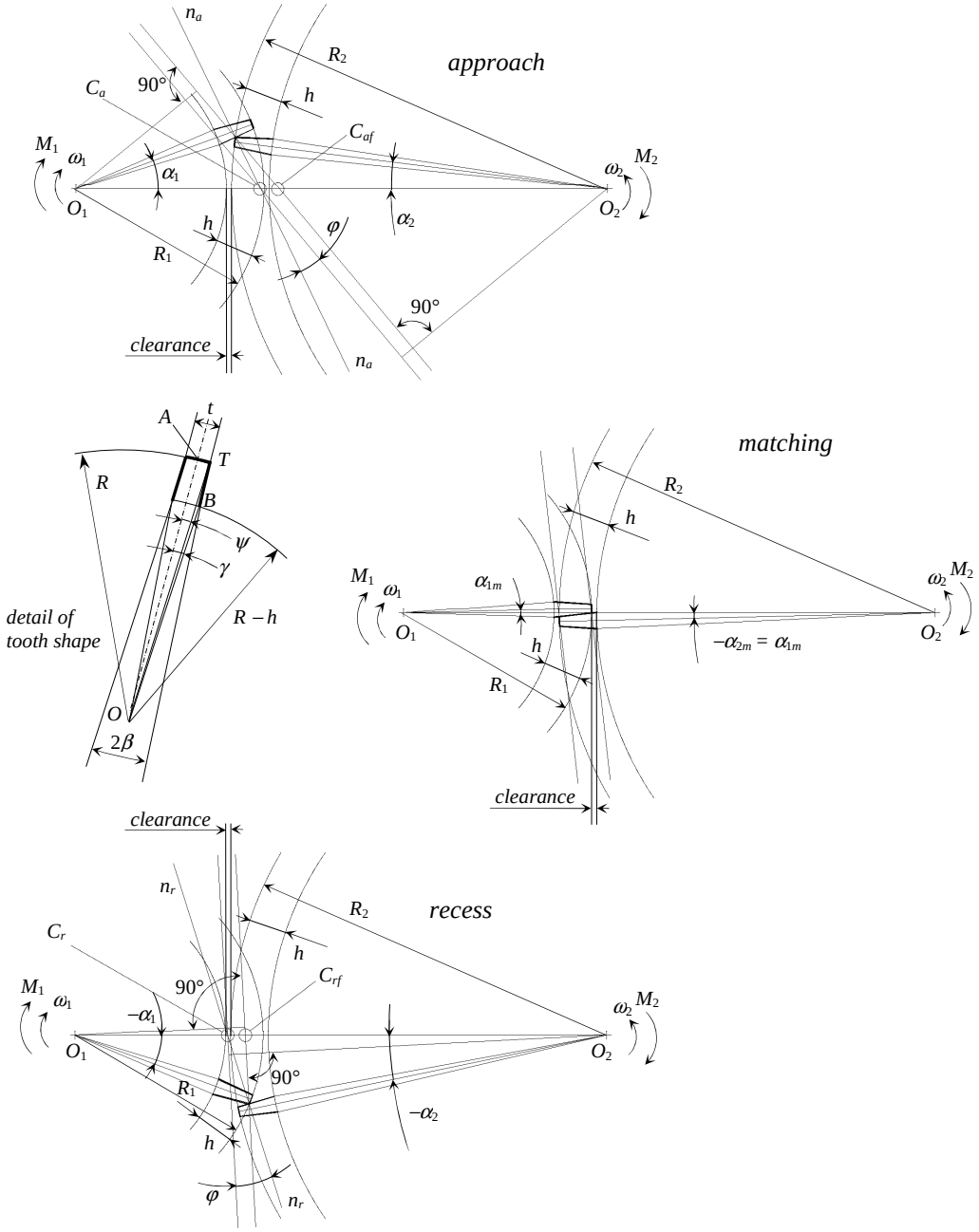


Figure 1: Scheme of tooth coupling.
$z_2/z_1 = 2$, $h/R_1 = 0.2$, $tz/(2\pi R) = 0.2$, $\beta = 5°$.

Rome by Marcus Claudius Marcellus after the conquest of Syracuse during the Second Punic War.

The gear technology was transmitted from the Hellenistic world to the Middle Ages, through

the Byzantine and Islamic culture, though largely loosing its original refinement, and gave origin to several machines, like odometers, calendars and clockworks. We also find gear devices in the codices of Leonardo da Vinci, i. e. at the dawn of the Modern Era, but the tooth shape has now turned rather rudimentary, often rectangular or trapezoidal, with some external rounding off at most, but far from the modern cycloidal or involute profiles developed after Euler [6,7].

This paper deals with the mechanical behavior of these primitive gear sets of the Middle Ages and the Renaissance. An approach similar to reference [8] will be applied.

## 2 GEOMETRY OF TRAPEZOIDAL TOOTHING

The scheme of the gear coupling is shown in Figure 1 for the three possible configurations: approach, matching and recess. The tooth number ratio can be considered as an average speed ratio, because of the variable position of the relative instant centre along the centre line during the mesh. According to the presumable design concepts of those days, it is assumed that the two gears have the same tooth tapering $2\beta$, the same depth $h$ from the tip to the root circle, the same thickness $t$ and the same circular pitch $p = 2\pi R/z$ on the outer circle, whence $R_1/z_1 = R_2/z_2$. Fixing the slenderness $h/p$, the total tooth number $z_{tot.} = z_1 + z_2$ and the mean speed ratio $z_1/z_2$, one gets $z_1$, $z_2$ and the tooth overhangs $h/R_i$. Then, referring to the detail of Figure 1, where $\psi = A\hat{O}T$, $\gamma = A\hat{O}B$, and applying the law of sines, one has

$$\frac{R_i}{\sin(\beta+\gamma_i)} = \frac{R_i - h}{\sin(\beta+\psi_i)} = \frac{e_i}{\sin(\gamma_i - \psi_i)} \tag{1}$$

where the subscript $i$ (= 1 or 2) refers to the driver or driven wheel. Since $t = 2R_i\psi_i$, the relations contained in Eqs. 1 permit calculating two of the three quantities $e_i/R_i$, $t/R_i$ and $\gamma_i$ as functions of the third one. Therefore, fixing the thickness-to-pitch ratio $t/p$, the gear geometry is completely defined save a scale factor (the gear mechanics is invariant with respect to the geometrical sizes).

The minimum center distance $D$ is $D_{min.} = R_1 + R_2 - h$, but an allowance factor $a$, a little greater than 1, has to multiply $D_{min.}$ necessarily in consideration of the unavoidable manufacturing inaccuracy of those days. Thus, $D = aD_{min.}$. After fixing the overall sizes ($D$), the maximum angular meshing width is specified by the intersections of the two tip circumferences:

$$\alpha_{1\ \substack{max.\\min.}} = \psi_1 \pm \arccos\left(\frac{D^2 + R_1^2 - R_2^2}{2DR_1}\right) \qquad \alpha_{2\ \substack{max.\\min.}} = -\psi_2 \pm \arccos\left(\frac{D^2 + R_2^2 - R_1^2}{2DR_2}\right) \tag{2 a,b}$$

## 3 MESHING KINEMATICS

Firstly, the engagement of a single tooth pair is analyzed, ignoring the preceding and following teeth. Then, the limits due to interference will be studied for sequential tooth gearings.

Starting from the initial meshing point at the upper intersection of the two tip circles of Figure 1, where the driver and driven profiles are in contact at their outer ends, an “approach” phase occurs, where the apex of the driven tooth is pushed by the side of the driver tooth, and then a “recess” phase, where the driver tooth apex pushes the side of the driven tooth, as far as the ending meshing point, at the lower intersection of the tip circles. The two phases are separated by the profile matching configuration, which occurs for $-\alpha_2 = \alpha_1 = \alpha_{1m} = -\alpha_{2m} > 0$ and we notice that the definitions of approach and recess are here slightly different from the modern gear terminology. The contact locus coincides with the arc of the driven tip circle preceding the matching position

$\alpha_{2m}$ plus the arc of the driver tip circle following the matching position $\alpha_{1m}$. The instant center of the relative motion is identifiable as the intersection of the center line and the normal to the active profile, of the driver wheel in approach ($n_a$) or of the driven one in recess ($n_r$). A sudden change of the speed ratio is expected at the passage from the matching position.

3.1 *Approach*

Two closure equations may be written

$$R_1\cos(\alpha_1-\psi_1)-v\cos(\alpha_1+\beta)+R_2\cos(\alpha_2+\psi_2)=D \tag{3}$$

$$R_1\sin(\alpha_1-\psi_1)-v\sin(\alpha_1+\beta)-R_2\sin(\alpha_2+\psi_2)=0 \tag{4}$$

where $v$ is the distance between the outer ends of the two profiles. Solving for $\alpha_2$ and $v$, one gets

$$\alpha_2(\alpha_1)=\arcsin\left[\frac{D\sin(\alpha_1+\beta)-R_1\sin(\beta+\psi_1)}{R_2}\right]-\alpha_1-\beta-\psi_2 \tag{5}$$

$$v(\alpha_1)=R_1\cos(\beta+\psi_1)-D\cos(\alpha_1+\beta)+\sqrt{R_2^2-[D\sin(\alpha_1+\beta)-R_1\sin(\beta+\psi_1)]^2} \tag{6}$$

The approach phase ends when $\alpha_2 = -\alpha_1$, whence Equation (5) yields

$$\alpha_{1m}=\arcsin\left[\frac{R_1\sin(\beta+\psi_1)+R_2\sin(\beta+\psi_2)}{D}\right]-\beta \tag{7}$$

The instant center $C_a$ of the relative motion and the speed ratio $\tau$ are obtainable by

$$\overline{O_2C_a}=\frac{\sqrt{R_2^2-[D\sin(\alpha_1+\beta)-R_1\sin(\beta+\psi_1)]^2}}{\cos(\alpha_1+\beta)} \tag{8}$$

$$\tau(\alpha_1)=\frac{\omega_2}{\omega_1}=\frac{D-\overline{O_2C_a}}{\overline{O_2C_a}}=\frac{D\cos(\alpha_1+\beta)}{\sqrt{R_2^2-[D\sin(\alpha_1+\beta)-R_1\sin(\beta+\psi_1)]^2}}-1 \tag{9}$$

3.2 *Recess*

Once passed the matching configuration, the closure equations become

$$R_1\cos(\alpha_1-\psi_1)-v\cos(\beta-\alpha_2)+R_2\cos(\alpha_2+\psi_2)=D \tag{10}$$

$$R_1\sin(\alpha_1-\psi_1)-v\sin(\beta-\alpha_2)-R_2\sin(\alpha_2+\psi_2)=0 \tag{11}$$

Solving for $v$ firstly and then for $\alpha_2$, it is possible to obtain

$$v(\alpha_1)=R_2\cos(\beta+\psi_2)-\sqrt{D^2+R_1^2-2DR_1\cos(\alpha_1-\psi_1)-R_2^2\sin^2(\beta+\psi_2)} \tag{12}$$

$$\alpha_2(\alpha_1)=\arctan\left\{\frac{\left[\frac{R_1\sin(\alpha_1-\psi_1)}{D-R_1\cos(\alpha_1-\psi_1)}\right]-\left[\frac{v\sin(\beta+\psi_2)}{R_2-v\cos(\beta+\psi_2)}\right]}{1+\left[\frac{R_1\sin(\alpha_1-\psi_1)}{D-R_1\cos(\alpha_1-\psi_1)}\right]\left[\frac{v\sin(\beta+\psi_2)}{R_2-v\cos(\beta+\psi_2)}\right]}\right\}-\psi_2 \tag{13}$$

The position of the instant center of the relative motion $C_r$ and the speed ratio may be derived as

$$\overline{O_1C_r}=\frac{R_1\cos(\beta-\alpha_1-\alpha_2+\psi_1)}{\cos(\beta-\alpha_2)} \tag{14}$$

$$\tau(\alpha_1)=\frac{\omega_2}{\omega_1}=\frac{\overline{O_1C_r}}{D-\overline{O_1C_r}}=\frac{R_1\cos(\beta-\alpha_1-\alpha_2+\psi_1)}{D\cos(\beta-\alpha_2)-R_1\cos(\beta-\alpha_1-\alpha_2+\psi_1)} \tag{15}$$

3.3 *Interference conditions*

Considering a generic contact point fulfilling the conditions of the previous subsections, either in approach or in recess, the angular distances of the homologous points belonging to the preceding and following teeth are $\pm 2\pi j/z_1$ and $\pm 2\pi j/z_2$ on the driver and driven gearwheel respectively ($j$ = 1, 2, …). Therefore, a point of the theoretical diagram $\alpha_2(\alpha_1)$ must be regarded as acceptable if and only if, tracing a straight line with slope $z_1/z_2$ through such a point, all other points whose abscissae differ by $\pm 2\pi j/z_1$ lie below the diagram, as otherwise there would be interference for some tooth pair. Actually, this condition ensures that all the other driven teeth are in advance than if they were in contact.

The diagram $\alpha_2(\alpha_1)$ exhibits a slight upward concavity nearly everywhere except at the matching position $\alpha_{1m}$, where a sudden slope change occurs. This is due to the fact that the speed ratio $d\alpha_2/d\alpha_1$ decreases during the course of each single phase and is subject to a step increase when passing through the matching configuration. Therefore, the no-interference condition leads to exclude all points of the full diagram that lie above the prolongation of that particular chord (or sum of aligned chords) with slope $z_1/z_2$ and projection (or sum of projections) $2\pi j/z_1$ on the $\alpha_1$ axis, that is altogether located as much as possible at the bottom of the plot concavity. The acceptable contact configurations, contained in the theoretical plot $\alpha_2(\alpha_1)$, may be identified by always checking the above no-interference condition for all preceding and following teeth.

As a matter of fact, this reasoning yields the practical conclusion that only one pair of profiles may be in contact at each time instant and, as soon as such profiles detach themselves, two new profiles join simultaneously to mesh, either of the following or of the preceding tooth pair, either upstream or downstream.

Assuming the tooth symmetry with respect to their axis and considering the inverse motion, it is clear that the new diagram $[\alpha_2(\alpha_1)]_{\text{inverse}}$ cannot but be symmetric of $\alpha_2(\alpha_1)$ with respect to the origin $\alpha_1 = \alpha_2 = 0$. As the position of the inactive profiles should fulfill the diagram $[\alpha_2(\alpha_1)]_{\text{inverse}}$ to be in contact, no interference occurs for them if all angles $\alpha_2$ of the following driven teeth are larger than if they were pushed in the inverse motion and all angles $\alpha_1$ of the preceding driver teeth are lower than if they were pushing in the inverse motion. In practice, shifting upwards the "direct" diagram $\alpha_2(\alpha_1)$ by $2\pi j/z_2$, all points must lie over the "inverse" diagram and, shifting it leftwards by $2\pi j/z_1$, they must lie left. This restrictions limit the tooth thickness, whose maximum

is reached when some inactive profile pair comes into touch. On this point, it is to be observed that the direct and inverse diagrams of the modern involute profiles are two straight segment symmetric with respect to the origin, away $2\pi j/z_1$ and $2\pi j/z_2$ from each other in the $\alpha_1$ and $\alpha_2$ directions. In theory, this coincides with the limit condition of interference, which is however eluded in practice by the well known tolerance between the thickness and space of the toothing.

### 3.4 *Transmission diagrams*

The theoretical contact diagram for one isolated pair and the acceptable plots for the sequential toothing are shown in Figures 2 a,b for two example cases.

Figure 2 a refers to a speed down case. The admissible portion of the diagram is confined in the approach region, differently from the triangular tooth case of [8], and its extent along the $\alpha_1$ axis is $360°/z_1$. As the diagram $\alpha_2(\alpha_1)$ shows a slight upward concavity, its admissible portion, i. e. compatible with the interference prevention, is confined under the bottom chord of width $360°/z_1$ and slope $z_1/z_2$. The speed ratio always decreases along the direction of the meshing evolution, i. e. from right to left, as the instant center of the relative motion always shifts towards the driving gear. The speed up case ($z_1 > z_2$) was not reported here for brevity, but is just similar to the speed down, save that the acceptable part of the diagram lies in the recess region. In both cases, on increasing the gearwheel allowance $a = D/D_{\text{min.}}$, the contact region moves towards the central position $\alpha_1 = 0$, until straddling the center for high $a$ values. In the meanwhile, the whole theoretical plot shrinks and the limit for the motion continuity is attained when one end of the theoretical region reaches one end of the admissible region. Clearly, the friction losses are lower when the contact region spreads in the close neighborhood of the central position, due to the lower sliding velocities, and thus, rather large clearances may improve the mesh conditions, while preventing the possible tooth locking with a sufficient margin.

In the case of equal gear radii and unit speed ratio on the contrary, if the wheel allowance is small, two partial meshing regions may be observed, the one in approach and the other in recess. The total width of these two sub-regions along the $\alpha_1$ axis is equal to $360°/z_1$, whose value is also equal to the distance between them. Therefore, indicating with the numbering, $j-1$, $j$, $j+1$, the sequence of three successive pairs of conjugate profiles and starting with the engagement of the pair $j$ in the approach sub-phase, from the right of the diagram towards the central position, the pair $j-1$ begins engaging in the recess sub-phase immediately after the conclusion of the approach sub-phase of $j$, and keeps on until the recess end. Then, the pair $j+1$ starts a new approach sub-phase from the right end and the whole process is repeated again. All this is possible because the distance between the two outer endpoints, on the right of the approach contact and on the left of the recess contact, is exactly equal to $2\times360°/z_1$.

On increasing the clearance, a third mesh sub-region appears around the matching position as shown in the example reported in Figure 2 b. In this case, the pair $j$ starts the approach sub-phase from the right of the diagram towards the centre, the pair $j-1$ begins the recess sub-phase immediately after the conclusion of the approach sub-phase of $j$ and afterwards the pair $j$ restarts a new engagement in the central sub-region after the recess end of $j-1$. After this last sub-phase, the pair $j+1$ starts a new approach sub-phase from the right end and the whole process is repeated again. On increasing the clearance further, the external sub-phases fade and a unique central phase remains, which straddles the matching configuration $\alpha_{1m}$ and lies in part in the approach region and in part in the recess one. Clearly the gearwheel clearance cannot be increased too much because we may get standstill period of the driven wheel, with important collisions at the new motion start, or else its definitive arrest.

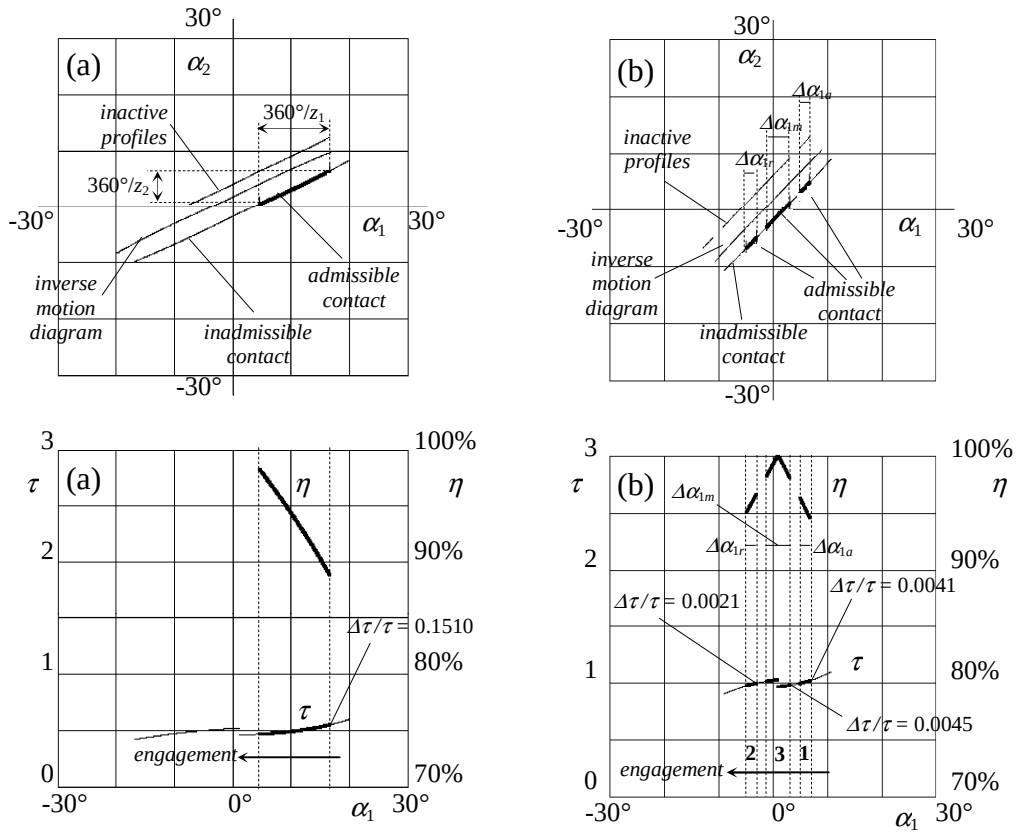


Figure 2 a,b: Driven gear rotation, efficiency and speed ratio as functions of driving gear rotation.

a) $h/p$ = 0.5, $\beta$ = 5°, $f$ = 0.25, $z_2$ = 60, $z_1$ = 30, $D/D_{\text{min.}}$ = 1.01, $t/p$ = 0.25

b) $h/p$ = 0.5, $\beta$ = 5°, $f$ = 0.25, $z_2$ = 45, $z_1$ = 45, $D/D_{\text{min.}}$ = 1.021, $t/p$ = 0.2
$\Delta\alpha_{1a}+\Delta\alpha_{1m}+\Delta\alpha_{1r} = 360°/z_1$, mesh sequence: 1, 2 (previous pair), 3

### 3.5 *Tooth collision*

The analysis of the previous sub-sections indicates that the speed ratio is always higher at the beginning of each mesh phase than at the end of the previous one, because the relative instant center always shifts towards the driver wheel center during each partial engagement. At the matching configuration furthermore, as the relative center is subject to a sudden displacement away from the driving gear, a step increase of the speed ratio occurs as well: indeed, all the intermediate points of the driven profile between the two tooth tips bounce on the driver profile, except the inner point, which remains in contact. Therefore, slight impacts take place at the beginning of each mesh phase or sub-phase, as the driven profile has a slightly lower speed before the engagement than after it.

Supposing that the impacts are inelastic, i.e. that, immediately after the conjunction of two profiles, the velocity components of the driver and driven points are equal along the normal to the contact, and assuming that the driver angular speed is constant, the relative impact velocity is given by $(v_{2\perp}^{+} - v_{2\perp}^{-}) / v_{2\perp}^{+} = 1 - \tau^{-}/\tau^{+}$ and the jump of the driven angular speed is proportional to the jump of the speed ratio.

Therefore, using the results of the previous subsections, it is possible to calculate all these sudden speed ratio jumps, in order to evaluate the extra work to be provided by the driver shaft for the step increases of the kinetic energy of the driven assembly.

All these speed jumps are of the order 10% and may produce a significant rattle of the gear system if the driving crank has an appreciable angular speed.

### 3.6 *Maximum tooth thickness*

Once fixed the profile shape, i.e. the tapering angle $2\beta$ and the tooth overhang $h/p$, on increasing the tooth thickness $t/p$ gradually, a condition is lastly reached where some interference between the inactive profiles begins. This limit condition and the maximum tooth thickness can be calculated as described in Section 3.3, shifting the direct motion diagram left and up by distances equal to the angular pitches of the driver and driven gears respectively, and comparing with the diagram of the inverse motion.

Some results are shown in Figure 3, fixing the sum $z_{tot.} = z_1 + z_2$ and varying the average speed ratio $z_1/z_2$. Each plot was traced for a different value of the allowance $a$ and it is clearly observable how the acceptable tooth thickness increases on increasing the allowance. Moreover, on increasing the tooth height $h$, larger clearances may be achieved, but with lower thickness for equal clearance. This may justify the tooth slenderness in the gearwheels of the Renaissance for remarkable overhangs.

## 4 TRANSMISSION LOSSES

Here, we only consider the losses ascribable to the tooth meshing. They are due to the sliding friction and to the tooth impact.

The ideal pressure angle, formed by the normals $n_a$ and $n_r$ to the active profile and to the center line, is $\beta + \alpha_1$ in the approach phase and $\beta - \alpha_2$ in the recess one, as deducible by Figure 1. Nevertheless, owing to the sliding friction, the line of action of the force exerted by the driver tooth on the driven one is rotated of the friction angle $\varphi = \arctan f$ with respect to the normal, towards the center of the driven wheel for almost every configuration of the meshing phases, both in approach and in recess (see Figure 1). Yet, in the close neighborhood of the matching position where the two straight flank touch each other and cross the center line, one may recognize a very short preceding interval, belonging to the approach region upstream, where $\alpha_2 + \psi_2 < 0$ and the contact point lies below the center line, and another very short following interval, belonging to the recess region downstream, where $\alpha_1 - \psi_1 > 0$ and the contact point lies above the center line. The sliding velocity has thus opposite direction in these two short sub-regions in comparison with the remaining larger main parts of the corresponding regions, of approach and recess respectively. As a consequence, the deviation of the line of action of the transmitted force is still equal to the friction angle $\varphi$ but now towards the driver gearwheel.

The distances of the force action line from the one and the other gear centers are the arms of the driver and driven moment and permit calculating the transmitted force itself because only one tooth pair is active at each time instant. It is supposed that the driver torque $M_1$ is known and constant, excepting the instantaneous peaks due to the tooth collisions.

The intersection of the force transmission line and the center line ($C_{af}$ in the approach phase and $C_{rf}$ in the recess phase) is calculable as

$$\overline{O_1 C_{af}} = D - R_2\left[\cos(\alpha_2 + \psi_2) - \sin(\alpha_2 + \psi_2)\tan(\beta + \alpha_1 + s_2\varphi)\right] \tag{16}$$

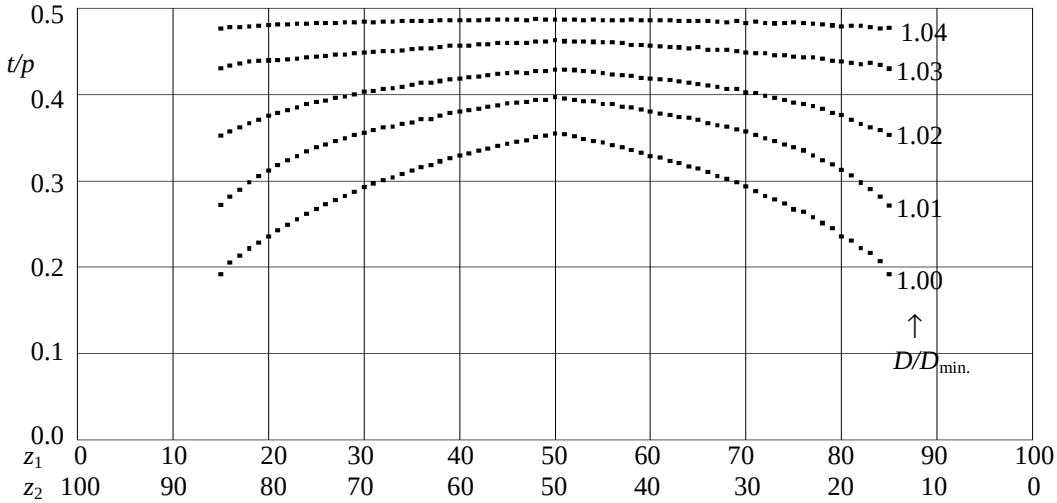


Figure 3: Maximum tooth thickness as a function of tooth number for various allowance levels.
Data : $h/p$ = 0.7, $\beta$ = 5°, $z_1 + z_2 = 100$

$$\overline{O_1C_{rf}} = R_1\left[\cos(\alpha_1 - \psi_1) + \sin(\alpha_1 - \psi_1)\tan(\beta - \alpha_2 + s_1\varphi)\right] \tag{17}$$

where the parameters $s_1 = \mathrm{sgn}(\alpha_1 - \psi_1)$ and $s_2 = \mathrm{sgn}(\alpha_2 + \psi_2)$ were introduced to consider the mentioned intervals of opposite sliding directions close to the matching position. Then, the arms $b_1$ and $b_2$ are obtainable multiplying the distance $O_1C_{af}$ and $O_2C_{af}$ by $\cos(\alpha_1 + \beta + s_2\varphi)$ in the approach phase, or multiplying the distance $O_1C_{rf}$ and $O_2C_{rf}$ by $\cos(\beta - \alpha_2 + s_1\varphi)$ in the recess phase. The torque applied to the driven gearwheel is $M_1 b_2 / b_1$ and is variable owing to the variability of the arms $b_1$ and $b_2$. Furthermore, this torque differs from the output resistant torque due to the secondary shaft inertia and the variability of $\omega_2$.

The efficiency $\eta_f$ due to the only sliding friction is obtainable as the product of the speed ratio $\tau$ and the arm ratio $b_2 / b_1$. The sliding friction energy loss during one complete meshing of two conjugate teeth can be calculated by integration. Figures 2 a,b also show the diagrams of the efficiency during the engagement for $f$ = 0.25, assuming bronze gearwheels and a sort of rudimentary lubrication, which somehow compensates for the necessarily crude profile finishing of the ancient times. As can be seen, the efficiency levels are as high as 90% - 100%, despite the primitive technology of those days.

Besides, the work $\frac{1}{2} J_2 \omega_1^2 (\tau_+^2 - \tau_-^2)$ must be provided by the driving wheel for every tooth collision, where $J_2$ indicates the moment of inertia of the driven wheel and all the other masses connected to the driven shaft, while the speed ratios $\tau$ refer to the instants immediately after and before the impact, to be calculated as previously described

The energy loss for each complete meshing phase is

$$E_{\text{lost per meshing phase}} = \sum_{\text{all sub-phases}} \int (1 - \eta_f) M_1 d\alpha_1 + \sum_{\text{all impacts}} \frac{1}{2} J_2 \omega_1^2 \left(\tau_+^2 - \tau_-^2\right) \tag{18}$$

where the integration is to be extended to all the mesh sub-phases of each tooth pair and the sum of the impact losses refer to all the impacts dividing such sub-phases.

## 5 CONCLUSION

The gear systems of the Middle Ages and the Renaissance, prior to the development of the cycloid and involute profiling, which has to be dated approximately from the Euler time, were sensibly coarse in comparison with the relevant advancement previously reached by the Hellenistic science, though all such gear mechanisms were characterized by the technology primitiveness of the ancient time. Nevertheless, an appreciable level of functionality can be detected by an accurate analysis. Differently from the modern gears, the ancient ones were certainly subject to a sensible rattle noise because of to the tooth collisions consequent to the variability of the speed ratio and its sudden changes when passing from the one the other engagement sub-phase. The energy losses were of course quite large in comparison with the present gear systems, but, guessing some rudimentary greasing or oiling of the contact even in the antiquity, the friction losses due to the rough technology of the tooth construction seems to be compensated in part by lubrication. The efficiency losses appear to be confined in a range of the order of 10% approximately.

*References*


[1] Pastore, G., *Il Planetario di Archimede Ritrovato* (The Discovery of Archimedes' Orrery), © Copyright 2006-2010 - Giovanni Pastore, www.giovannipastore.it, ISBN 9788890471520 (in Italian).

[2] De Solla Price, D.J., "An ancient Greek computer," *Scientific American*, 200, 6, 60-67 (1959).

[3] De Solla Price, D.J., "Gears from the Greeks. The Antikythera Mechanism: A Calendar Computer from ca. 80 B. C.," *Transactions of the American Philosophical Society*, new series, 64, 7, 1–70 (1974).

[4] Wright, M.T., Bromley, A.G. and Magkou, E., "Simple X-ray Tomography and the Antikythera Mechanism," *PACT, Revue du groupe européen d'études pour les techniques physiques, chimiques, biologiques et mathématiques appliquées à l'archéologie* (Journal of the European Study Group on Physical, Chemical, Biological and Mathematical Techniques Applied to Archaeology), 45, 531–543 (1995).

[5] The Antikythera Mechanism Research Project, http://www.antikythera-mechanism.gr., March 23, 2007.

[6] Leonardo da Vinci, *The Madrid Codices*, I, f. 5, f. 116, (1493-1495).

[7] Moon, F.C., *The Machines of Leonardo da Vinci and Franz Reuleaux: Kinematics of Machines from the Renaissance to the XX Century*, Springer (2007).

[8] Sorge, F., "A note on the mechanics of ancient gear systems," *13th IFToMM Congress*, Guanajuato, Mexico, June 20-22, 2011.